Experimental search for the electron Electric Dipole Moment using solid state techniques

Y. J. Kim[1,a], C.-Y. Liu[1,b], S. K. Lamoreaux[2], G. Reddy[1]
[1] Indiana University, Physics Department, Bloomington, IN 47408, USA
[2] Yale University, Physics Department, New Haven, CT 06520, USA

E-mail: [a]yjk2@indiana.edu, [b]cl21@indiana.edu

Abstract. We report results of an experimental search for the permanent Electric Dipole Moment (EDM) of the electron using a solid state system. The experiment uses a paramagnetic insulator (gadolinium gallium garnet) with a large magnetic response at low temperatures. The presence of the electron EDM leads to a finite magnetization when the garnet sample is subjected to a strong electric field. The resulting magnetization can be measured using a superconducting quantum interference device (SQUID) as a magnetometer. With considerable efforts made towards controlling various sources of systematic effects, the experiment is currently free of spurious signals larger than the SQUID noise. We report the value of electron EDM of $(-5.57 \pm 7.98 \pm 0.12)\times 10^{-25}$e·cm with 120 hours of data.

1. Introduction

A search for the permanent electric dipole moment (EDM) in fundamental particles is motivated to test the Standard Model (SM) of particle physics [1]. For an electron, its EDM vector (if exists) must align with the spin vector to avoid any additional degeneracy in the system. Because of the different transformation properties under discrete symmetry operation from that of the spin, the EDM requires the physical laws governing the electron to violate both the time reversal (T) and the parity (P) symmetries. While the theory of parity violation has been firmly established with numerous experimental evidences, the studies of EDM would provide information about the nature of the less well understood T violation. T violation has only been observed directly in the neutral-kaon [2] and more searches in the B system are underway [3]. On the other hand, provided that the CPT theorem is valid, T violation implies CP violation, which is extensively studied in the high energy experiments. Using the known CP violation in the CKM matrix, the SM predicts the electron EDM (d_e) to be at 10^{-38}e·cm level, which is well beyond the reach of the current experimental techniques [4]. New sources of CP violation beyond the SM often lead to a sizable EDM, that can be compared with experimental constraints. Free from the SM backgrounds, measurements of EDM present as a powerful way to test various extensions to the SM, including the very popular supersymmetric models, that generate EDM of fundamental particles comparable to the current experimental limit. Even though none of the experimental efforts have yielded positive results, the EDM searches over the past decades have ruled out many theoretical models. With ever-more-refined experimental techniques, EDM searches continue to be of fundamental significance in particle and nuclear physics [5].

The leading experimental technique used to measure EDM is based on the nuclear magnetic resonance; EDM interactions induce a shift in the Larmor precession frequency when the fermion

is under an externally applied electric field, in addition to a magnetic field. In the past few years, we have been pursuing an alternative approach, in the attempt to improve the experimental limit of the d_e, using a non-conventional solid state technique first reported in [6, 7]. In this paper, we will explain the solid state method and describe efforts to control systematic effects and improve the sensitivity. The major efforts include the design and implementation of a 24-bit data acquisition (DAQ) system with ultra-low degrees of channel crosstalks, and the control of the high voltage drift. With these, we report our first background-free experimental limit of d_e.

2. Experimental method

The idea of applying the solid state system to search for the d_e was first proposed by Shapiro [8]. In the presence of a strong electric field, the EDMs of the unpaired bound electrons inside an insulating paramagnet align with the E field. Because the EDM vector is bound to the direction of the spin vector, a non-zero net EDM alignment results in a net electronic spin polarization of the sample. The spin ordering generates a bulk magnetization which produces a magnetic field surrounding the paramagnetic sample. Due to the small energy of EDM interactions, the induced magnetic field is minute. However, the magnetic signal could accumulate among a large number of electrons inside the solid. Using a modern magnetometer such as a superconducting quantum interference device (SQUID), one can detect this EDM-induced magnetic flux manifested by the Stark aligned d_e. The measured change in the magnetic flux coupled to the SQUID sensor, $\Delta\Phi_{sq}$, is given by

$$\Delta\Phi_{sq} = \beta f \cdot \frac{\chi \alpha d_e E}{\mu_a} \cdot A \tag{1}$$

where χ is the magnetic susceptibility of a sample, α is the EDM enhancement-related factor in the sample, E is the applied electric field, A is the area of the pickup coil, and μ_a is the magnetic moment of the paramagnetic ions in the sample. In addition, β is the flux loss factor when the flux picked up from the sample is delivered to the SQUID and f is the flux suppression factor due to the demagnetizing effect depending on the sample geometry. Because of the relativistic effects, electrons in high atomic shells experience an enhanced electric field, the atomic EDM of large Z atoms would have larger overall EDM that scales with Z^3, where Z is the atomic number, than that of the bare electron [9]. With all considerations outlined above, the ideal sample to apply the solid state technique is a paramagnetic insulator containing high Z elements to increase the sensitivity to the d_e. In this experiment, we chose a Gadolinium Gallium Garnet (GGG) paramagnetic insulator. The GGG has superb dielectric strength of 10 MV/cm and seven unpaired electrons on the $4f$ shell of Gd ions which lead to a strong magnetic response. It also has a high number density of Gd ions ($\sim 10^{22}\mathrm{cm}^{-3}$) containing unpaired electrons. Detailed calculations involving atomic and crystal fields [10, 11, 12, 13] indicate that the measured atomic EDM signal per Gd ion in the GGG structure in the internal field corresponds to 2.97 times the bare d_e in the applied field, hence the EDM enhancement-related factor α in the GGG sample is 2.97 (Note that the reduction of the internal field due to the dielectric constant has already been account for in the calculations). To enhance the measurable flux, we would also need a strong external field, a large sample size and an optimized magnetic flux pickup coil. To extract d_e from the EDM-induced magnetic flux, we need to experimentally determine the paramagnetic susceptibility of the GGG sample.

3. Experimental setup and results

We measured the magnetic susceptibility χ of the synthesized GGG sample using a SQUID susceptometer system (Quantum Design MPMS). The result is shown in Fig. 1 in the log scale from 295 K to 2 K. The data confirms the typical paramagnetic behavior of the GGG sample in which χ increases with decreasing temperatures. The Curie-Weiss fit ($\chi = \frac{C}{T-\theta_{CW}}$) gives the Curie-Weiss temperature of -2.1 K, which indicates that adjacent Gd ions have intrinsic

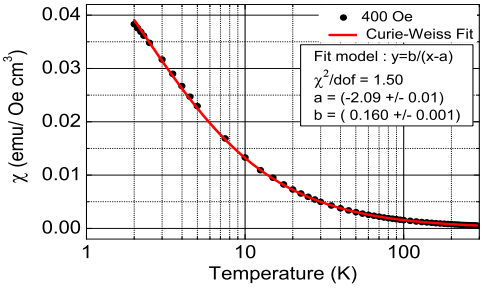

Figure 1. χ vs. temperature in log scale. The black circle points correspond to the volume χ and the red line to the Curie-Weiss fit.

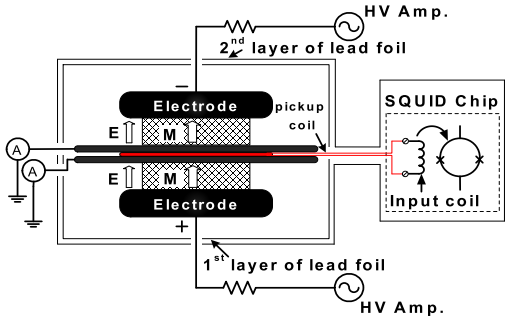

Figure 2. An schematic experimental setup for measuring the magnetic flux from the GGG sample.

antiferromagnetic (AF) coupling. The strong AF coupling would lead to a order-disorder phase transition at low temperatures that could limit the size of χ. For the GGG, the phase transition was highly suppressed due to the geometric frustration in the triangular lattice. To maintain a high sensitivity to d_e, we need the spins to remain free. To further suppress the spontaneous magnetization, we have attempted to spin dilution. The substitution of magnetic Gd ions with non magnetic Y ions considerably decreases strength of AF interactions in the system, resulting in a smaller Curie-Weiss temperature and possibly lower phase transition temperatures.

As shown in Fig. 2, the experiment consists of two disk-shaped GGG samples with a diameter of 1.3 in, a height of 0.3 in, and a density of 6.66 g/cm^3 inserted between two planar electrodes and two isolated ground plates. In between the ground plates is the flux pickup coil in the form of a planar gradiometer which integrates the flux produced by the sample and more importantly eliminates the common mode residual magnetic signal inside the magnetic shield. The gradiometer is optimized to enhance the magnetic flux by partially enclosing the returning flux with the current enhancement factor of 1.1 (estimated using a finite element analysis calculations). The effective area for flux pickup A in the Eq. (1) would be 1.1 times the actual area of the pickup coil (This factor would increase up to 1.8 by shrinking the radial dimension of the superconducting lead shield). The pickup coil is inductively coupled to a low temperature DC SQUID sensor (Superacon CE2blue, with an input coil inductance of 420 nH and a mutual inductance between input coil to SQUID of 8.1 nH). With an inductance of the pickup coil of 618 nH, the flux loss factor β in Eq. (1) is estimated to be 0.0078. The electrodes are made of ceramics coated with graphite. The large electrical resistivity helps to reduce eddy currents and magnetic noise measured by the SQUID sensor. During the measurements, high voltages (HV) of opposite polarities are applied to the two HV electrodes so that the electric fields in both samples are in the same direction. The leakage currents on the ground plates are monitored with separate current amplifiers. The assembly of GGG samples and electrodes is shielded using two layers of superconducting Pb foils and additional three layers of mu-metal (Metglas alloy ribbon) in the x, y, and z directions. The experiment is contained inside a helium cryostat and immersed in a bath of liquid helium at atmospheric pressures. Finally, one layer of Co-Netic cylinder at room temperature is used to enclose the whole vacuum chamber to provide initial reduction of the ambient fields.

The flux suppression factor f of the disk-shaped sample with a 1.3 in diameter and a 0.3 in height is calculated using a finite-element analysis calculations. The solution shows an non-uniform magnetic field given a uniform magnetization inside the disk-shaped sample. The magnetic flux is suppressed by a factor of 0.369 due to the demagnetization effect of the finite geometry, and another factor of 0.425 due to the placement of the pickup coil (that is 0.13 in

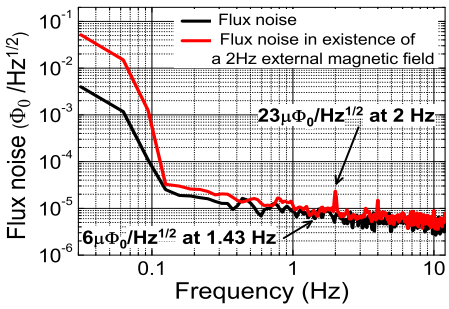

Figure 3. The flux noise spectrum of the SQUID sensor.

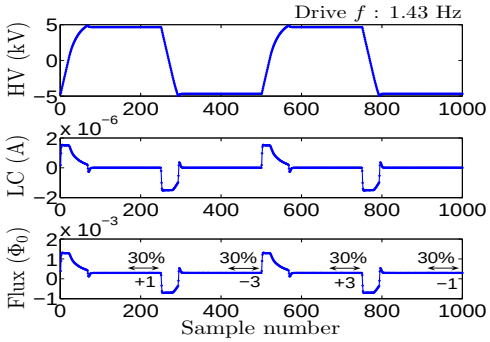

Figure 4. Averaged signals over 3 hours using the 24-bit DAQ system.

away from the surface of the sample). The total flux suppression factor f in Eq. (1) is 0.157. Note that this suppression factor can be improved by having the pickup coil closer to the sample for future experiments.

Because the expected magnetic signal detected by the SQUID sensor is very small, possible signal contamination by other voltage and current monitoring channels is detrimental. To address this problem, we built a high precision 24-bit DAQ system with the intrinsic rms noise of 1.38 μV which consists of a master board and eight individual ADC boxes. Each ADC box is individually shielded with a heavy-duty RF shielding enclosure to minimize any channel crosstalks (better than 191 dB). To maintain stable operation of the SQUID sensor at the base noise level, any uncontrolled sources of electromagnetic interference (RFI) are undesirable. Considerable effort went into studying and eliminating (if possible) any sources that generate electrical RF noise in the lab, and eliminating ground loops. As shown in Fig. 3 (black curve), the baseline of the SQUID sensor is $6\mu\Phi_0/\sqrt{Hz}$ at the frequency of operation, after significant improvements (over a factor of 50) on the RFI reduction and the magnetic shield. The red curve is the spectrum with an application of a 2 Hz external uniform magnetic field of 10 Gauss. By comparing the amplitude of the residual 2 Hz signal to the applied field strength, we estimate the overall magnetic shielding factor of the system to be 5×10^{11}. It also worths pointing out that the flux noise spectrum does not show any obvious vibrational peaks or 60 Hz harmonics which is a major achievement in itself.

During the experiment, we applied voltages of alternating polarities up to $\sim$10 kV$_{pp}$ (full capacity of the supply) using a square waveform with finite-sloped ramps between field reversals. The polarity switching cycle is repeated at a rate of 1.43 Hz. The drive frequency is chosen to be low enough to minimize the displacement currents, but high enough to avoid the $1/f$ corner on the SQUID noise spectrum (see Fig. 3). Using the 24-bit DAQ system, we monitored high voltages (through 1000:1 voltage dividers), currents flowing in the ground plates, and the magnetic flux on the SQUID sensor. A typical 3 hours data-taking gives an averaged waveform shown in Fig. 4. Since the EDM-induced flux aligns with the direction of the applied electric field, the relative change of the measured flux between the two HV polarity plateau should be proportional to the EDM signal.

Despite all the improvements described above, there still exist residual voltage drifts in SQUID electronics. To remedy this, a drift-corrected algorithm that subtracts signals between adjacent two cycles of the field reversal (+1 -3 +3 -1) is applied to the d_e calculation where the drift function (as a polynomial function) up to the second order can be eliminated. The transient regions right after each field reversal are excluded in the calculation. The Gaussian fit of the distribution of the flux difference within each polarity cycle, collected over 3 hours

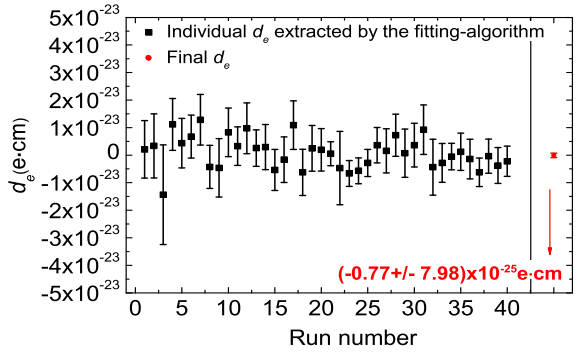

Figure 5. Distribution of individual d_e and the final d_e value with proper error-weighting.

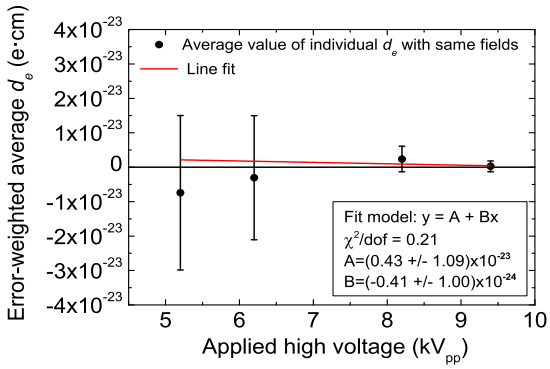

Figure 6. Error weighted average d_e with same fields vs. high voltages.

of measurements, gives the $\Delta\Phi_{sq}$ of (-1.89±9.25)×$10^{-8}\Phi_0$, which corresponds to the d_e of (-0.24±1.17)×10^{-23}e·cm (after taking into accounts of all the suppression factors mentioned above). We also use a fitting algorithm that fits the averaged readout of the SQUID sensor under one cycle for 3 hours on each HV polarity with a voltage model of $V = Ae^{-t/\tau} + Bt + d$. The first term in the model characterizes the decay of the transient displacement current with the time constant τ, the second term is the voltage drift on the SQUID electronics, and the constant term d represents voltage changes due to EDM interaction. The model fit gives the $\Delta\Phi_{sq}$ of (3.07±6.34)×$10^{-8}\Phi_0$, which corresponds to the d_e of (0.39±0.81)×10^{-23}e·cm. The higher sensitivity of the latter method of analysis compared with the former method is because the fitting algorithm uses about 2.5 times more data points than the drift-corrected algorithm. We collected data over two weeks, with a total data integrating time of 120 hours. Analysis using the two methods has similar distributions of the extracted d_e, and we show the results using the fitting-algorithm in Fig. 5. Each black data point (each run) lasts for three or four hours. Proper error-weighting is applied to sum the results of runs to arrive at the final d_e value of (-0.77±7.98)×10^{-25}e·cm. This results could be compared with the previous experimental limit using a complimentary solid-state method in gadolinium iron garnet system [14].

A comprehensive list of systematic effects is shown in Table 1. Since the measured physical observable is the magnetic flux, we compare the spurious flux generated by each known systematic effect. The dominant one is the leakage current through the sample which produces a magnetic field in phase with the polarity of the HV. To the first order, the magnetic field generated by the leakage current is perpendicular to the EDM-induced magnetization, some fraction of the field, however, can be measured by the SQUID sensor due to the tilt of the pickup coil. Surface currents forming a helical path would generate additional magnetic flux. Studies on the correlation between the leakage currents, the time derivative of the high voltages, and the SQUID signal show that about 0.014 of the radial field generated by the the leakage current could leak into the pickup coil and contributes to the spurious field. For example, a leakage current of (6±2) pA (averaged over 3 hours) measured at the maximum applied voltage generates the spurious magnetic flux Φ_{sq} of (3.79±1.26)×$10^{-9}\Phi_0$. In addition, we show in Fig. 6 the averaged d_e with different applied E fields (most measurements were made at 9.4 kV$_{pp}$). The results indicates that the d_e is independent of the strength of the applied field within the error bars, suggesting that the experiment is free of systematic effects related to the HV. This significant improvement is achieved by developing an ultra-low distortion HV supply with 10 ppm/sec of voltage drift (by a factor of 600 over the previous supply) with improving the feedback circuits in the HV tube amplifier. We also attempted to characterize the magnetic hysteresis of the GGG

Table 1. Systematic effects

Origin	$\Delta\Phi_{sq}$	Comments
Currently measured	$(0.48 \pm 6.02) \times 10^{-9}\Phi_0$	Averaged over all runs
Displacement current	$1.65 \times 10^{-10}\Phi_0$	$C\frac{dV}{dt}$ <0.2 pA at 9.4 kV_{pp}
Leakage current	$(3.18 \pm 0.07) \times 10^{-9}\Phi_0$	Averaged over all runs
		$< 2.19 \times 10^{-8}\Phi_0$
Remanent Magnetization	$< 6.02 \times 10^{-9}\Phi_0$	Limited by the direct MPMS measurements
Channel cross-talks	$(0.52 \pm 1.51) \times 10^{-10}\Phi_0$	Channel isolation > 191 dB
Vibrational peaks at the field reversal frequency	$< 6.02 \times 10^{-9}\Phi_0$	

sample using the SQUID-based susceptometer, however due to the variations of the residual field upon every field ramping, the system cannot determine the magnetic hysteresis of the GGG sample to the level comparable to the magnetic measurements carried out in our EDM experiment. Since there is no non-zero offset between the half cycles, we place an upper limit of the remanent magnetization using our EDM result. Given the magnetic susceptibility, we need to control the remanent magnetization (that changes with applied field) to be smaller than 2.5×10^5 Bohr magneton/cm^3. Using Eq. (1), we calculate the correction due to the total systematic effect is (-4.80±0.12)$\times10^{-25}$e·cm. This leads to the final reported eEDM value of (-5.57±7.98_{stat}±0.12_{syst})$\times10^{-25}$e·cm with 120 hours of data.

4. Conclusion and perspective

In this experiment, we demonstrate the feasibility of the solid state method using the GGG paramagnetic insulator at 4 K for the d_e search with the report of the first background-free result. Further enhancement of the sensitivity using the GGG system is possible. It would require cooling the experiment at sub-Kelvin temperatures using a dilution refrigerator. At such low temperature, the spin ordering would increase according to 1/T behavior of the paramagnetic susceptibility. In addition, we plan to scale up the system by factor of 10, increase electric fields to 40 kV_{pp} and employ a better SQUID sensor with lower noise. With these improvements, we expect to push the sensitivity comparable to and beyond the most sensitive experiment using the atomic beam method [4].

References

[1] E. M. Purcell and N. F. Ramsey 1950 *Phys. Rev.* **78**, 807
[2] CPLEAR Collaboration 1998 *Phys. Lett.* B **444** 43
[3] Ezequiel Álvarez and Alejandro Szynkman 2008 *Mod. Phys. Lett.* A **23** 2085
[4] B. C. Regan, E. D. Commins, C. J. Schmidt, and D. DeMille 2002 *Phys. Rev. Lett.* **88** 071805
[5] N. Fortson, P. Sanders, and S. Barr 2003 *Phys. Today* **56** 33
[6] S. K. Lamoreaux 2002 *Phy. Rev.* A **66** 022109
[7] C.-Y. Liu and S. K. Lamoreaux 2004 *Mod. Phys. Lett.* A **19** 1235
[8] F. L. Shapiro 1968 *Sov. Phys. Usp.* **11** 345
[9] P. G. H. Sandars 1965 *Phys. Lett.* **14** 194
[10] S. Y. Buhmann, V. A. Dzuba, and O. P. Sushkov 2002 *Phys. Rev.* A **66** 042109
[11] T. N. Mukhamedjanov, V. A. Dzuba, and O. P. Sushkov 2003 *Phys. Rev.* A **68** 042103
[12] V. A. Dzuba, O. P. Sushkov, W. R. Johnson, and U. I. Safronova 2002 *Phys. Rev.* A **66** 032105
[13] S. A. Kuenzi, O. P. Sushkov, V. A. Dzuba, and J. M. Cadogan 2002 *Phys. Rev.* A **66** 032111
[14] B. J. Heidenreich, O. T. Elliott, N. D. Charney, and *et al* 2005 *Phys. Rev. Lett.* **95** 253004